Atmospheric Environment 319 (2024) 120261



Contents lists available at ScienceDirect

Atmospheric Environment

journal homepage: www.elsevier.com/locate/atmosenv

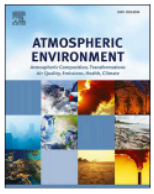



Validating CFD modelling of ship plume dispersion in an urban environment with pollutant concentration measurements

Christos Boikos [a], Panagiotis Siamidis [a], Sonia Oppo [b], Alexandre Armengaud [b], George Tsegas [a], Johan Mellqvist [c], Vladimir Conde [c], Leonidas Ntziachristos [a,*]

[a] Mechanical Engineering Department, Aristotle University of Thessaloniki, GR 54124, Thessaloniki, Greece
[b] AtmoSud, Air Quality Observatory in the Provence-Alpes-Côte D'Azur Region, FR 13006, Marseille, France
[c] Department of Space, Earth and Environment, Chalmers University of Technology, SE 41320, Göteborg, Sweden

HIGHLIGHTS

- Harbour-scale steady RANS-CFD modelling for plume dispersion of pollutants emitted from ships.
- CFD assesses ship plume dispersion in ports and cities down to 2.5 m resolution.
- Predicted pollutant concentrations deviate 8.2% from observed levels at the 80th percentile, 250 m downwind of the vessel.
- Steady-state solution proposed to reliably capture ship pollution incidents while reducing computational cost.
- Tool suitable to assess the effectiveness of reduction measures for exposure to ship pollution.

ARTICLE INFO

Keywords:
Shipping emissions
Harbour
Air quality
RANS-CFD
FLUENT
Validation

ABSTRACT

Air pollution in urban areas constitutes a global environmental problem, with shipping being one major contributor to hazardous pollutants in harbour areas. This work concerns the application of a method using CFD modelling to study how ships affect the air quality of port areas at a microscale level. A steady RANS-CFD approach was applied to simulate the dispersion of shipping-emitted pollutants, and a spatial sensitivity analysis of the CFD modelling results was conducted. The port of Marseille was used as a case study, and the CFD predictions were compared with on-site observations from two monitoring stations for CO_2, CO, NO_x, SO_2 and PM concentrations. Representative modelled and measured concentrations were considered at the location of the monitoring stations to facilitate one-by-one comparisons for all pollutants in three different test cases of departing vessels. The modelling predictions presented an 8.2% (95% CI: -9.3%, 25.7%) average deviation from the measurements. Validation metrics were included to conduct a statistical comparison between predicted and measured concentrations, with almost all metric values indicating acceptable agreement between the CFD model and measurements. From a technical perspective, this study demonstrates the reliability of the applied CFD modelling method in estimating shipping plume dispersion, while from a societal perspective, this model can serve as an advisory tool for port authorities and policy makers to reduce the impact of shipping emissions on urban air quality.

1. Introduction

Increased urbanization rate has led to densely populated urban areas. It is estimated that by 2050 over 80% of the global population will be residing in big urban areas (United Nations, 2018). In 2020, 96% of the European Union (EU) urban population was exposed to fine particulate matter ($PM_{2.5}$) that exceeded the health-based guideline level established by the World Health Organization (WHO), resulting in up to 238,000 premature deaths (EEA, 2022). The transport sector, including shipping, was a major contributor in ambient air pollution, being responsible for 44%, 21%, and 11% of NO_x, CO, and PM_{10} emissions, respectively, in the EU in 2020 (EEA, 2022).

Lately, there has been a systematic effort to study the impact of shipping emissions on the air quality, in particular coastal areas (Karl et al., 2019; Matthias et al., 2010). It was estimated that the annual

* Corresponding author.
E-mail address: leon@auth.gr (L. Ntziachristos).

https://doi.org/10.1016/j.atmosenv.2023.120261
Received 19 June 2023; Received in revised form 31 October 2023; Accepted 26 November 2023
Available online 2 December 2023
1352-2310/© 2023 Elsevier Ltd. All rights reserved.

Abbreviations

AFR	Air-to-Fuel Ratio
AIS	Automatic Identification System
CFD	Computational Fluid Dynamics
CI	Confidence Interval
CO	Carbon Monoxide
CO_2	Carbon Dioxide
ECA	Emission Control Area
EF	Emission Factor
FSC	Fuel Sulphur Content
IMO	International Maritime Organization
LHV	Lower Heating Value
NO_2	Nitrogen Dioxide
NO_x	Nitrogen Oxides
PM	Particulate Matter
RANS	Reynolds-Averaged Navier–Stokes
RKE	Realizable k-epsilon turbulent model
SFOC	Specific Fuel Oil Consumption
SKE	Standard k-epsilon turbulent model
SO_2	Sulphur Dioxide
VSP	Virtual Sampling Point

average contribution of shipping emissions in the Mediterranean and the North Seas is 1–7% for PM_{10} and 7–24% for NO_2 (Viana et al., 2014). For the reduction of shipping emissions, the International Maritime Organization (IMO) has set new regulations. For the reduction of Particulate Matter (PM) and Sulphur Oxides (SO_x) emissions, vessels should use fuel with less than 0.1% (m/m) sulphur content within Emission Control Areas (ECAs) since January 1st, 2015, and less than 0.5% (m/m) for non-ECAs since January 1st, 2020 (IMO, 2016). Limits have been also set for Nitrogen Oxides (NO_x) based on rated engine speed classes (rpm) and construction date of vessels (IMO, 2014).

The assessment of vessel emissions' impact on the air quality of port areas and their surrounding urban environments is often done by installing an air quality monitoring network within a shipping-affected urban area (Toscano et al., 2022). To properly capture the spatial distribution of vessel plumes, a rather large monitoring network should be installed which is expensive and cumbersome as suitable and available locations in a city landscape are scarce. Furthermore, the contribution of shipping to air pollution cannot always be isolated from the overall observed signal. To fill this gap, air quality dispersion models have been developed to estimate pollutants concentration in urban environments. Pan et al. (2021) developed a regional-scale plume dispersion model representing ships as moving point emission sources. NO_2 and $PM_{2.5}$ concentrations were predicted on a 1 km × 1 km plane grid with a 100 m × 100 m nested sub-grid and 10–500 m vertical layering. Compared to earlier modelling approaches, such model's predictions better agreed with observations, especially for the area close to the emission sources. Li et al. (2022) conducted a parametric study regarding ship plume rising of individual moving vessels, using the computational fluid dynamics (CFD) model PHOENIX. They produced two parametric equations for exhaust funnel temperature and velocity to correct results produced from stationary-ship approach simulations. They suggest that this correction can be potentially applied to correct the results from mesoscale models. Badeke et al. (2021) deployed the microscale chemistry, transport, and stream model MITRAS, to parametrically investigate downward plume dispersion considering an individual vessel. It was found that wind speed and ship size strongly influence downward dispersion. A remarkable outcome was that for high lateral wind speed conditions, the inclusion of the whole vessel structure in their model led to 25% more downward dispersion. Rapkos et al. (2023) used CFD modelling to reproduce the plume dispersion of individual vessels crossing the Elbe River near Hamburg, Germany. The objective of this work was to correlate the Fuel Sulphur Content (FSC) of the vessels with the on-shore SO_2 concentration estimated from the CFD model or measured by a monitoring station to identify any possible regulatory violations of the FSC limit. Toscano et al. (2021) studied the shipping emissions impact on the air pollution of a coastal area, using the Lagrangian and Gaussian puff dispersion model CALPUFF and a RANS-CFD model, and then compared their results with wind tunnel experiments at different receptor points. Wind tunnel experiments were better reproduced by the CFD model while the CALPUFF model systematically underestimated the time-averaged concentrations at the ground level.

Recently, much research has focused on studying the plume dispersion of shipping emissions. Badeke et al. (2021), Li et al. (2022) and Rapkos et al. (2023) studied the plume dispersion in the vicinity of individual vessels, but not considering the dispersion within the urban area. For the studies where microscale modelling in urban environments was applied, mainly Gaussian models have been used. According to Tominaga and Stathopoulos (2016), considerable inaccuracies may arise in areas where complex geometries, such as urban areas, and wind flows prevail, which cannot be adequately captured by Gaussian-based plume models. In contrast, CFD models can adequately simulate air flows in various urban applications (Blocken, 2015; Blocken and Gualtieri, 2012; Du et al., 2021), and on higher resolution compared to larger-scale air quality models. Additionally, only few works have been validated or compared either with already validated models or with on-site measurements.

Regarding air pollution, ships can be modelled as substantial quasi-point emission sources, which can potentially lead to locally excessive exposure in specific areas within an urban port environment. This combined with the presence of three-dimensional structures like buildings and street canyons that increases turbulent wind patterns, directly influences the dispersion of ship-generated plumes. To deal with such air pollution problems, Computational Fluid Dynamics (CFD) emerges as the most suitable tool. This study aims for the first time to provide a method for applying and validating a RANS CFD model that has been developed to investigate the impact of shipping emissions on the air quality of urban environments adjacent to ports. The port of Marseille was used as a case study. To validate the CFD model, the predicted concentrations of CO_2, CO, NO_x, SO_2, and PM were compared to the corresponding measured concentrations from two air quality monitoring stations inside the port of Marseille. By utilizing the CFD model, decision-makers can identify pollution zones inside the city highly affected by ship emissions, prioritize emission reduction strategies, and assess their effectiveness in various scenarios. Furthermore, the model's insights into wind airflow patterns can inform urban planning efforts, promoting air quality improvements and minimizing the exposure of vulnerable populations to pollutants emitted by ships.

2. Methods

2.1. Port of Marseille and measurement campaign

The port of Marseille was used as a case study in order to validate the air quality dispersion model. The port of Marseille can be separated into two main areas, the cruise ship and the ferry boat (Ro-Ro) ones (Fig. 1a), with the current work focusing on the latter (Fig. 1b). The buildings included in the model concern an area of approximately 2 × 1.2 km^2, in which plumes from departing, arriving, and hoteling vessels can be characterized by low dilution and elevation levels. The boundaries of the modelled area are the waterfront south and east and major urban highways at the north; extending the area north-bound would reduce the contribution from vessels due to the strong signal from urban traffic. The tallest building in this area is La Major Cathedral with its rooftop being 75 m above sea level.

In July 2021, a measurement campaign took place in the studied area

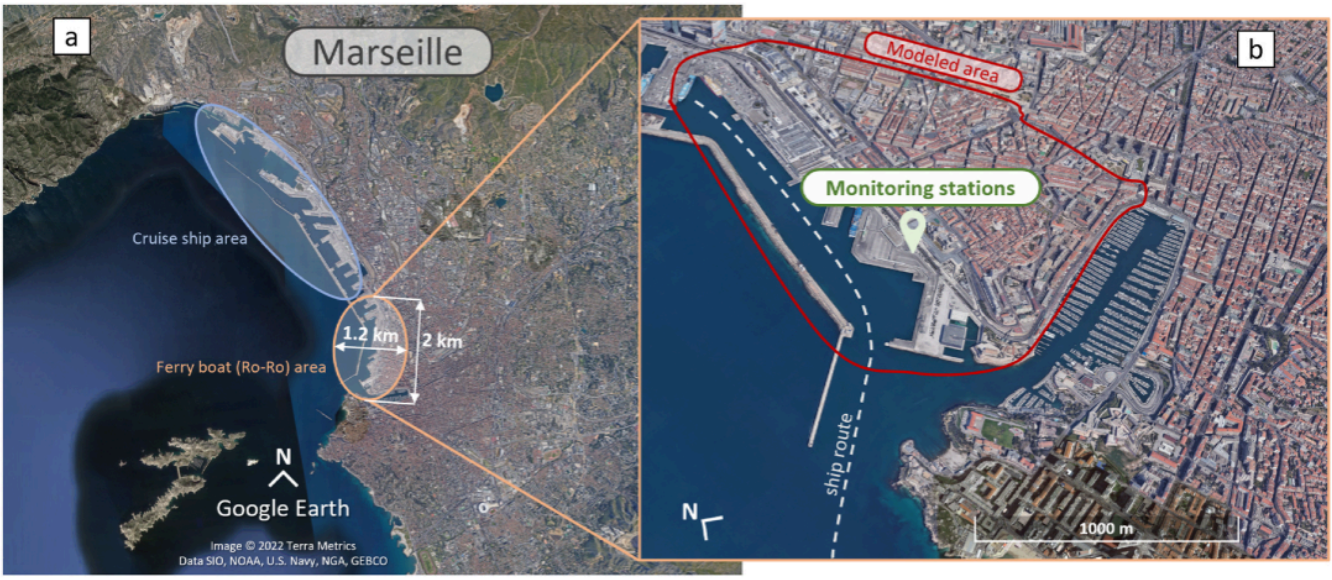

Fig. 1. (a) Berthing areas at the port of Marseille; (b) Studied area (ferry boat) and location of air quality monitoring station. Source: Google Earth.

(Fig. 1b) as part of the Horizon 2020 SCIPPER project. Two monitoring stations were installed at Lat: 43.300020°, Lon: 5.363382°, with a 7-m distance to each other. Both stations recorded SO_2, NO_x, CO, and CO_2 concentrations, and only one station PM, on a 24/7 basis for 15–20 days. The temporal sampling period was 1–10 s for all pollutants, except for PM which was obtained with 1-min resolution. Wind speed and wind direction were also recorded. During the campaign, ship trajectories were obtained from Automated Identification System (AIS) data. Then, each detected signal was matched to the corresponding vessel, combining AIS data and prevailing wind conditions.

2.2. Computational domain

The computational domain is defined as the space surrounded by the four cardinal boundaries (North, West, South, and East), the free flow plane (top layer), and the bottom layer. The bottom layer consists of the

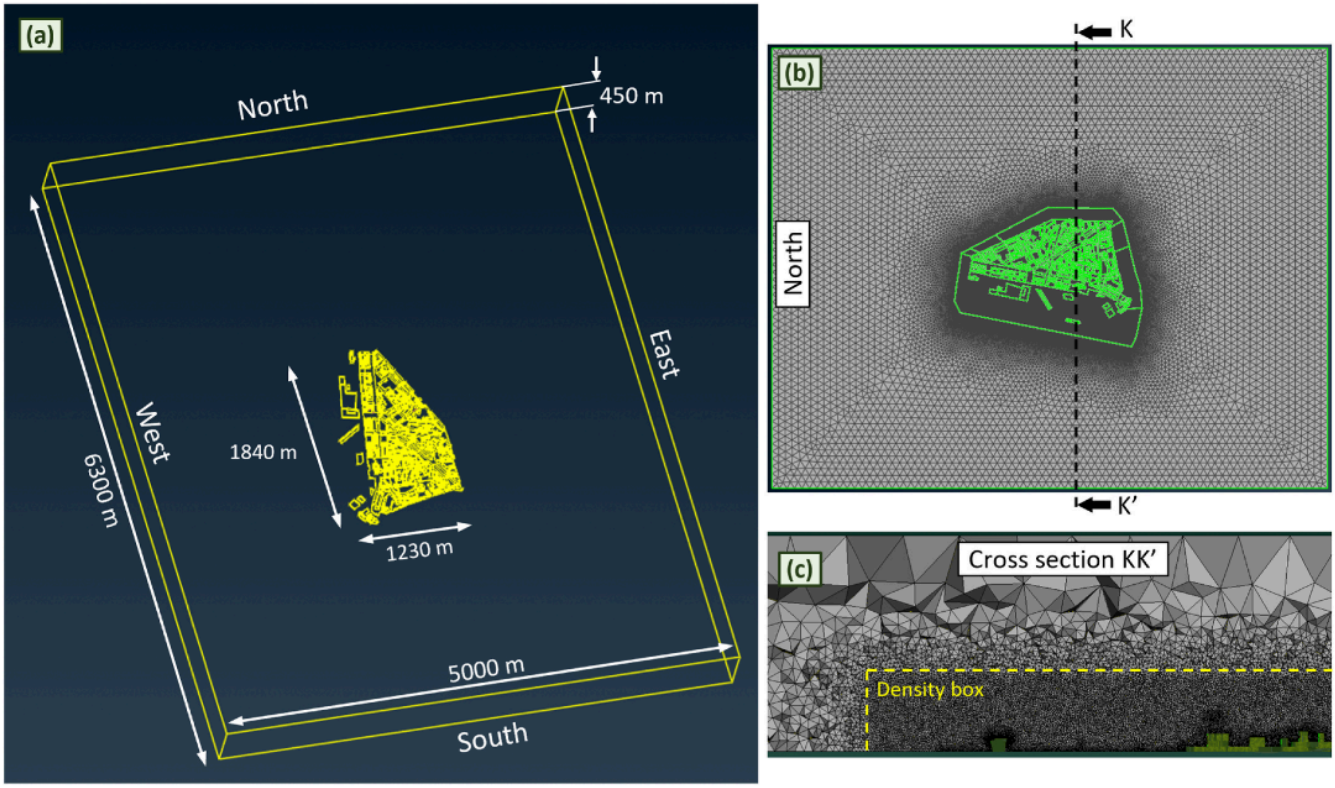

Fig. 2. Computational domain of the CFD model. (a) Domain dimensions compared to the size of the modelled area; (b) Top view of surface tetrahedral meshing; (c) Cross section KK' of volume mesh, showing the density box around the area of interest.

ground, the seawater surface, and the external surfaces of buildings and vessels. The creation of the domain included the detailed geometric representation of vessels as well as of the buildings in the surrounding port area. The size of this area is 1840 × 1230 m^2 (Fig. 2a). In CFD studies regarding urban flows, the computational domain should be several times bigger than the modelled area. This additional space acts as a buffer zone, ensuring that the flow is no longer affected by the presence of the buildings close to the boundaries. Blocken (2015) points out that artificial flow acceleration may appear if the side and the top layer faces of the computational domain are not located far enough from the 3D objects, such as buildings and vessels. For this reason, it is proposed that the blockage ratio (BR) in each direction, defined as the ratio of the total length of the buildings over the total domain length in the specific direction, should be lower than 17% $\left(BR_L = \frac{L_{building}}{L_{domain}} \leq 17\%\right)$. Franke (2006) states that the outflow boundaries should be placed 15 times away from the height of the highest building (H_{max}). According to Blocken (2015) and Franke (2006) the domain size of the current study should be 10.8 × 7.2 km^2 and 4.1 × 3.5 km^2, respectively. The selected domain size is 6.3 × 5 km^2 (Fig. 2a), which is between these two alternative recommendations. The selection of this size was, again, a compromise between model accuracy and computational efficiency. In any case, no artificial acceleration of the airflow close to the non-physical boundaries (side and top layers) was observed. As for the domain height, the rule of 6•H_{max} proposed by Tominaga et al. (2008) was followed. The height of the tallest building is 75 m, leading to a 450 m computational domain height.

The surface mesh of the CFD model was built using triangular cell elements with a 1.12 growth rate (Fig. 2b). The volume mesh consists of tetrahedral unstructured elements, with maximum skewness equal to 0.9 (Fig. 2c). Furthermore, a mesh sensitivity study was conducted, ending up in a meshing with 41 million tetrahedral volume cells. For the selected mesh, the cell size was set at 2.5 m on the buildings and the surrounding to them surfaces, while the vessel funnel surface had a 0.2–0.4 m cell size, due to its finer geometry. For the density box, shown in Fig. 2c, the maximum volume cell size was limited to 5 m, assuring higher resolution in the area where the plume is mainly dispersed.

2.3. CFD numerical model

The current study was conducted using the commercial software ANSYS Inc, 2021 R1. RANS CFD modelling was applied, where quantities like velocity are distinguished in two terms. The first one is the average part, stating the magnitude of the quantity, and it is discretized and resolved based on a numerical method. The second is the variable part, which states the variability or turbulence of the main quantity. This part is resolved with a turbulence modelling approach. Ricci et al. (2020) studied the impact of different turbulence models in 3D steady RANS simulations within urban environments. Their predictions better agreed with wind tunnel experiments, when k-epsilon turbulence models, such as standard k-epsilon (SKE) and realizable k-epsilon (RKE), were adopted. Santiago et al. (2013) and Amorim et al. (2013) applied CFD modelling to study the dispersion of traffic-oriented pollutants in urban centers, and they, also, adopted the k-epsilon turbulence model. Prior studies have shown that the turbulence models belonging to the k-epsilon family can properly model the turbulence of the airflow within an urban environment. Hence, in the current work, the standard k-epsilon (SKE) turbulence model is selected, as it belongs to the k-epsilon family.

Wang and Wang (2019) studied the effect of noise barriers on the dispersion of traffic-emitted pollutants in highways and they found that the non-reacting species transport model (ANSYS FLUENT 19.2) best matched with the experimental data. Li et al. (2016) studied the impact of roadside vegetation barriers on the dispersion of traffic emissions. For the dispersion of carbon monoxide, they adopted the same species transport model, showing acceptable agreement with field observations. Based on this previous experience, the same species transport module of FLUENT (ANSYS Inc, 2021 R1 Theory Guide, 2021) was applied to simulate the dispersion of shipping emissions. In the species transport model, the gas mixture consists of two gases, the carrier air and the pollutant one, with each one having separate flow properties.

A critical aspect that complicates the application of CFD modelling is the chemical processes that occur in the atmosphere. The pollutants considered in the current work are NO_x, SO_2, CO and PM_{tot}, while the time scale of the studied events was smaller than 10 min. NO_x is typically defined as the sum of NO and NO_2. This consideration is also included in the methodology for calculating the NO_x emission factors (Grigoriadis et al., 2021). Sanchez et al. (2017) applied CFD-RANS modelling to trace NO_x dispersion from road traffic emissions in an urban hot-spot area. They considered NO_x as a non-reactive pollutant, as the NO–NO_2–O_3 reaction scheme does not affect the balance of NO_x concentration. The modelling results exhibited satisfactory agreement with the field measurements. Long et al. (2017) state that the SO_2 reaction with OH is critical for clarifying the fate of SO_2 in the atmosphere. For altitudes lower than 5 km a typical time scale of the SO_2–OH reaction is 196 h. Additionally, Jaffe (1968) states that *"the mean residence time of CO (τ_{co}) in the lower atmosphere has been variously estimated to be between 0.3 years to < 5 years"*. Holmes and Morawska (2006) state that in simplified dispersion models the mass conservation principle for PM is generally adopted. This means that the total PM concentration is not affected by the aerosol dynamic processes such as coagulation and condensation. Given that air quality regulations are based on particle mass concentrations and not particle number concentrations, simplified models can adequately model PM dispersion, especially for short distances and averaging periods. Blocken et al. (2016) apply CFD modelling to study the removal capability of PM in semi-enclosed parking garages. Similar to our study, they adopted this simplified approach for the PM treatment. Hence, it is safe to conclude that the pollutants under investigation are chemically inert, either because of the short studied time scales compared to the reaction time scales (for CO and SO_2), or due to the balance in pollutant concentrations (for NO_x and PM_{tot}).

The studied funnel exhaust gases are Carbon Dioxide (CO_2), Carbon Monoxide (CO), Nitrogen Oxides (NO_x), Sulphur Dioxide (SO_2), and Particulate Matter (PM). A diffusion coefficient is needed for the species transport model. The diffusion coefficients of the selected pollutants range from 10^{-9} (PM) to 10^{-5} m^2/s (rest of pollutants), which is several orders of magnitude lower than the turbulent diffusivity (or eddy viscosity, ~10^{-1} m^2/s) close to 3D obstacles (Bonifacio et al., 2014). Thus, within an urban environment, the pollutants are primarily diffused due to the production of turbulence and secondarily due to their diffusion. Based on this, an average diffusion rate equal to 1.2×10^{-5} m^2/s was set for all pollutants, creating a proportionality between source emission rate and pollutant concentration. Regarding buoyancy effects, the Oberbeck-Boussinesq approximation was applied, as no atmospheric temperature gradients were considered (Mayeli and Sheard, 2021).

For the calculation of boundary wind conditions, the Lagrangian model PMSS (Parallel-Micro-SWIFT-SPRAY) model was used (Oldrini et al., 2019). PMSS is a combination of the PSWIFT and PSRAY sub-models, developed and distributed by ARIA Technologies. PSWIFT produces the 3D wind components (U, V, W), using observations from a network of meteorological stations in the studied area while taking into account any 3D obstacles. PSPRAY is the dispersion model which estimates the concentration of gaseous pollutants in the atmosphere. The PMSS model has its own computational grid and mathematical background that differ from the CFD model. For the purposes of this study, the vertical profiles of wind components (U, V, W), produced by PMSS with a 1-min resolution for each cardinal point (North, East, South, West), were averaged and used as input boundary conditions at the boundaries of the CFD model. An example of the estimated vertical wind profiles by the PMSS model is showcased in Fig. 3. In this example, the average estimated wind direction is northwest (312°), signifying that wind enters the CFD domain through the Northern and Western

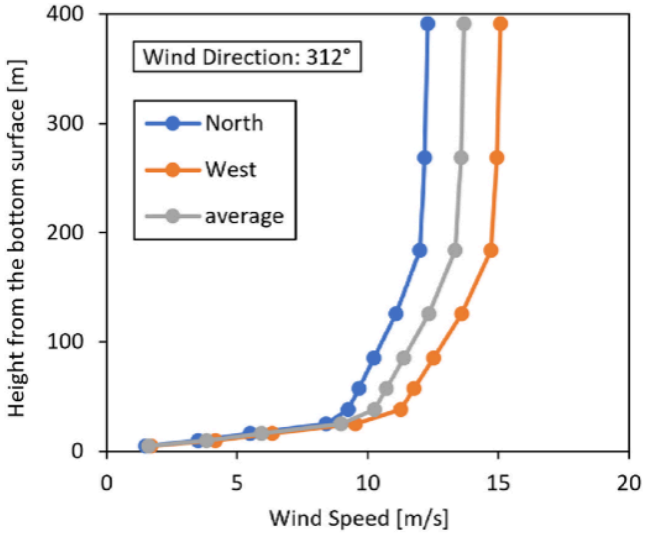

Fig. 3. Indicative vertical wind profile calculated by the PMSS at the North and West boundaries of the CFD model. The wind is of the northwest direction (312°). Blue: average profile for the North boundary; Orange: average profile for the West boundary; Light gray: average profile for both North and West boundaries (used in the CFD).

boundaries. The vertical wind profiles at these boundaries are represented in blue and orange colors, respectively. To ensure numerical stability, the average wind profile (light gray color) is selected as the input for both the Northern and Western boundaries in the CFD simulation. The average profile is then automatically interpolated from the CFD code to align with the nodes of the CFD computational mesh.

Another important process during the setup of a CFD simulation is the implementation of the boundary conditions. For each one of the boundaries, a separate boundary condition was set.

- Bottom layer: Velocity on these surfaces was set equal to zero (no-slip wall boundary condition).
- Cardinal point boundaries (North, East, South, West): Depending on the prevailing wind direction, two of the sides work as wind inflows and the other two as outflows. For the former, a vertical wind profile calculated from the PMSS model was set, while for the latter pressure was set equal to 1 atm.
- Top layer: The symmetry boundary condition was selected, meaning that no exchange between the two sides of the boundary is allowed.
- Vessel funnel: The mass flow rate for the exhaust gases and the pollutant in [kg/s], were uniformly set.

2.4. Emissions modelling

To calculate the total exhaust gases mass flow at the ship funnel, the air-to-fuel ratio (AFR) was set to 29 (2 times more than the stoichiometric ratio), the Lower Heat Value (LHV) of the fuel was considered 43.4 [MJ/kg] and the exhaust funnel temperature T_{exh} = 380 K. These assumptions were made based on still unpublished measurements in the exhaust system of an on-board marine engine. Ntziachristos et al. (2016) state that AFR may exceed 40 in marine diesel engines. Haugen et al. (2022) used an air quality model to simulate the dispersion of passenger ship emissions, assuming that the air-to-fuel ratio and the exhaust funnel temperature are equal to 28–30 and 320–350 K, respectively. Their assumptions are of the same order of magnitude as the ones made for this work. Then, the total exhaust mass flow rate ($\dot{m}_{exh,tot}$) is calculated as it is presented in Eq. (1) and Eq. (2), and the emission rate (ER) for each pollutant in Eq. (3). SFOC is the specific fuel oil consumption during the combustion, and P_{dem} is the power demand from the vessel. The emission factors (EFs) for each pollutant were calculated based on the methodology described by Grigoriadis et al. (2021).

$$\dot{m}_{exh,tot}\left[\frac{kg}{s}\right] = (AFR+1)\cdot\dot{m}_{fuel}\left[\frac{kg}{s}\right] \quad \text{Eq. 1}$$

$$\dot{m}_{fuel}\left[\frac{kg}{s}\right] = \frac{SFOC\left[\frac{MJ}{kWh}\right]\cdot P_{dem}[kW]}{LHV\left[\frac{MJ}{kg}\right]}\cdot\frac{1[h]}{3600[s]} \quad \text{Eq. 2}$$

$$ER\left[\frac{g}{s}\right] = P_{dem}[kW]\cdot EF\left[\frac{g}{kWh}\right]\cdot\frac{1[h]}{3600[s]} \quad \text{Eq. 3}$$

2.5. Proposed validation method

The purpose of this work is the application of a modelling approach to simulate singular ship emissions and their plume dispersion in a port area. The simulation outcome is a 3D high-resolution map where the concentration of ship-originated pollutants is quantified within the urban canopy. Fig. 4a is a graphical representation of a vessel navigating on a designated route adjacent to an urban area, while its plume moves towards the urban vicinity. This might be a typical incidence of an arriving or departing vessel at a port. The detailed reproduction of such a situation with a CFD model would demand increased computational resources. Specifically, a transient analysis would be needed, where the vessel position and the mesh around it should change at each time.

To simplify the approach and take the concentration which is most representative from an air-quality point of view, we only solve for a steady-state solution when the vessel is optimally placed to obtain the highest plume concentration at the measurement station (Fig. 4b). In Fig. 4b this optimal location is defined as the representative vessel position, where the plume is directed straight to the monitoring station, representing the incidence of Fig. 4a. Based on this approach, a compromise between the increased computational demands of an accurate simulation, and the cost efficiency of a simpler but representative approach is achieved.

Next, to account for the geometrical uncertainty in the exact position of the monitoring stations within the modelling domain (grid cell size of 4.6 m compared to the 7 m distance of the measurement stations), we considered the spatial average concentration of the x-y-z surrounding grid cells to the location of each station. This average simulated concentration is then compared to the average of the s-by-s values within the 80th highest percentile of observations for the particular plume incidence (Fig. 4), in order to obtain a better statistical representativity than comparing only to the single highest observation.

2.6. Validation test cases

To evaluate the CFD model, the proposed validation method is applied. Specifically, the predicted concentrations are compared with the observed values in the case of three plume incidents while vessels departed from the port of Marseille. Table 1 presents the vessels' attributes and their pollutant emission rate as well as the wind boundary conditions for each case. The method described by Grigoriadis et al. (2021) was applied to calculate the emission factors (EFs) for each pollutant. Based on this method, the EFs are a function of the engine size, load and fuel used. Engine load depends on the vessel category and its operating phase (hoteling, manoeuvring, cruising). In the selected cases, all vessels are Roll on/Roll off (Ro-Ro) ones and the plume incidences take place during manoeuvring in departure. In this phase, the engine load for the main and the auxiliary engines was set at 20% and 21.4%, respectively. The main engine power of the vessels was derived from the free database of FleetMon, 2023. In U.S. EPA (2009) it is estimated that the auxiliary to main engine power ratio for the Ro-Ro vessel category is 0.259. This ratio was used to calculate the auxiliary engine power in

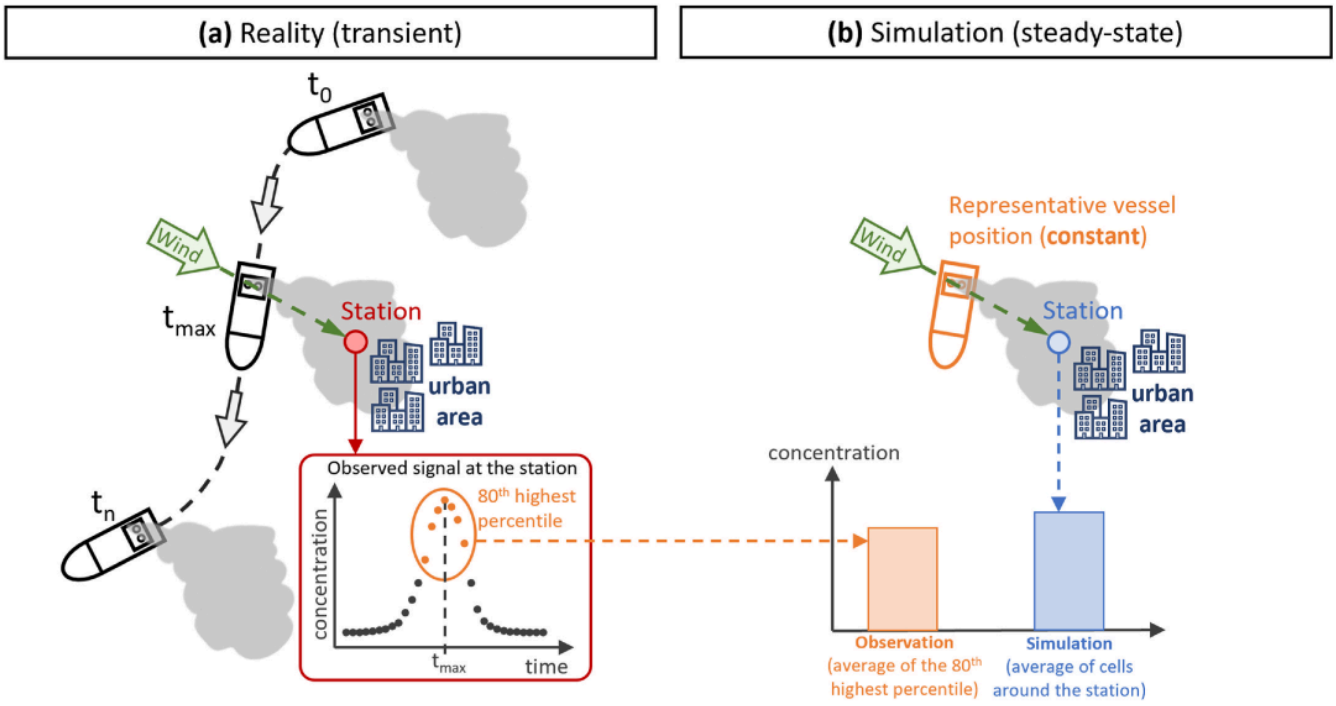

Fig. 4. Graphical representation of a moving vessel in front of an urban area. (a) A real incident of a vessel navigating on a designated route and the corresponding observed concentration signal of the pollutant from a monitoring station; (b) Steady-state modelling approach (fixed vessel position) where the vessel is located in the most representative position. Comparison of average observed (orange) and predicted (blue) concentration.

Table 1
Vessel attributes, prevailing wind conditions and pollutant emission rates for the three test cases used for the validation of the CFD model.

Vessel Type		Case 1	Case 2	Case 3
		Ro-Ro/Passenger		
Engine Power [MW]	Main	19.7	38.4	19.7
	Auxiliary	5.1	9.9	5.1
Ship length [m]		165.8	180	165.8
Ship width [m]		29	31	29
Exhaust funnel area [m^2]		2.73	5.6	2.73
Average funnel height [m][a]		36.9	33.7	36.9
Exhaust gases temperature [K]		380	380	380
Exhaust gases mass flow [kg/s]		13.3	21.6	13.3
Exhaust funnel velocity [m/s]		5.24	4.15	5.24
Fuel Sulphur Content (% S m/m)		0.445	0.578	0.356
Wind boundary conditions	speed at 10 m above bottom surface [m/s]	3.50	0.93	0.87
	direction [deg]	312	285	250
Average peak duration [min][b]		2.5	2	3
Estimated vessel speed [m/s][c]		4.3	4.6	4.4
Ship emissions [kg/s]	CO_2	1.14 E+00	1.49 E+00	1.13 E+00
	CO	3.21E-03	5.21E-03	3.21E-03
	NO_x	1.75E-02	3.28E-02	1.75E-02
	SO_2	3.10E-03	6.57E-03	2.45E-03
	P_{mtot}	6.85E-04	1.19E-03	6.32E-04

[a] Average distance of funnels from the sea level.
[b] How long a concentration peak lasts based on the measurements.
[c] Calculated from the available AIS data.

Table 1. Fuel sulphur content (FSC) in each case was calculated based on observed data during the ongoing measurement campaign with the method described by Balzani Lööv et al. (2014).

To give a better insight to the reader regarding these plume incidents it is critical to provide some indicative measurement data concerning the monitoring stations. Fig. 5 presents the concentration time series for all pollutants detected by monitoring station 2 during the Case 2 incidence. For comparability reasons, the axes limits were adjusted properly for each pollutant in the graph. The average background concentration during the measurement campaign for the CO_2, CO, NO_x, SO_2 and PM_{tot} was 414 ppm, 162 ppb 15.4 ppb, 0.64 ppb and 12.2 μg/m^3, respectively. A peak in all pollutants signal is observed between 19:22 and 19:24. This timeframe coincides with the passage of a particular vessel in front of the stations, as indicated by the AIS data. The observed peak is distinctively higher than the average background concentration for all pollutants. Given the sea-oriented wind and the fact that no other pollution source intervenes between the vessel and the two stations, these peaks can only

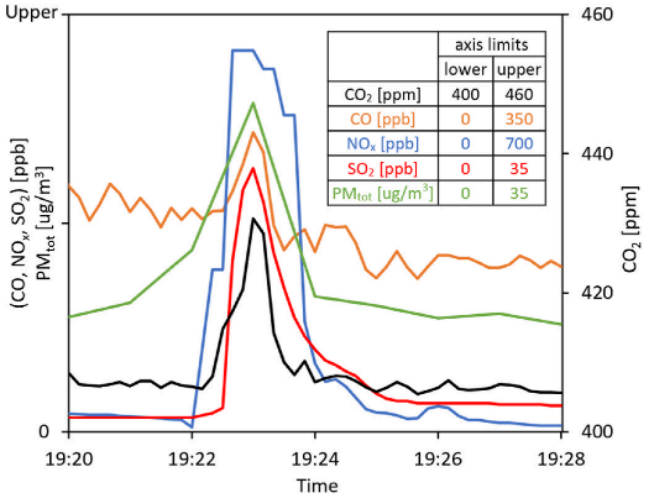

Fig. 5. Concentration signals of CO, NO_x, SO_2, PM_{tot} (left axis) and CO_2 (right axis) during the Case 2 incidence detected by monitoring station 2.

be attributed to the presence of this specific vessel (Case 2). The average wind speed and wind direction at station 2 during this period were measured at 1.94 m/s (95% CI: 1.79 m/s, 2.10 m/s) and 300° (95% CI: 295°, 304°), respectively. Similar behaviour was observed in Cases 1 and 3.

3. Results

3.1. Plume dispersion results and spatial sensitivity of the CFD model

The main output of the plume dispersion CFD model is a three-dimensional map of pollutant concentration. To better understand how the plume is dispersed we need first to analyze the wind patterns produced by the interaction of the 3D obstacles with the air flow. In Fig. 6, Fig. 7, Fig. 8, and Fig. 9 the results for Case 2 of Table 1 are presented, considered indicative of the CFD output. Fig. 6a presents the contour plot of the wind speed magnitude on a plane parallel to the plume direction, and vertical to the sea surface, crossing the vessel's funnel. A low wind speed area is observed within the first 150–200 m downwind of the vessel, up to the vessel's funnel stack, indicating a low ventilation level. Fig. 6b presents the vertical distributions of wind speed and wind direction in the vicinity of the monitoring stations. The vertical profiles are divided into two sub-areas, the physical boundary of which is the rooftop of the neighbouring building (La Major Cathedral). The first area concerns heights above the rooftop where the wind has a smooth transitional behaviour, while the second one is below this physical limit, and both wind speed (WS) and wind direction (WD) are characterized by strong variability. The presence of buildings creates pressure gradients that affect the airflow, increasing the turbulence and affecting the dispersion of pollutants in this area.

Fig. 7 illustrates the pressure and the vertical wind velocity component fields on the same plane as depicted in Fig. 6 providing better insights on the downwind plume evolution originating from the vessel. In Fig. 7a, the vertical wind speed component is depicted, with positive values denoting upward airflow and negative indicating downward flow. Within the first 150–200 m downwind of the vessel a region of negative vertical velocity is observed. This phenomenon can be attributed to the development of a low-pressure zone on the vessel's leeward side (Fig. 7b). At approximately the height of the funnel stack and above, a zone of positive velocity area is created, favoring the upward movement of the plume. In Fig. 7c the gauge pressure (defined as the difference between total pressure and atmospheric pressure) along the P_1–P_2 line of Fig. 7b is plotted. An over-pressure area is created upwind of the vessel, which is followed by an under-pressure region on its downwind side. These spatially sharp changes in both pressure and wind velocity are caused by the presence of the vessel, highlighting the suitability of CFD as an appropriate tool for such plume transport studies within highly turbulent port environments.

Fig. 8 shows the vessel of Case 2 during its departure from the port of Marseille and the dispersion of the resulting SO_2 plume. The vessel has a fixed representative location, where the plume is carried directly towards the La Major Cathedral (the tallest building in the vicinity) due to the prevailing wind conditions. The average height of the ship's funnel is 37 m above sea level and corresponds to point A. The plume is depicted

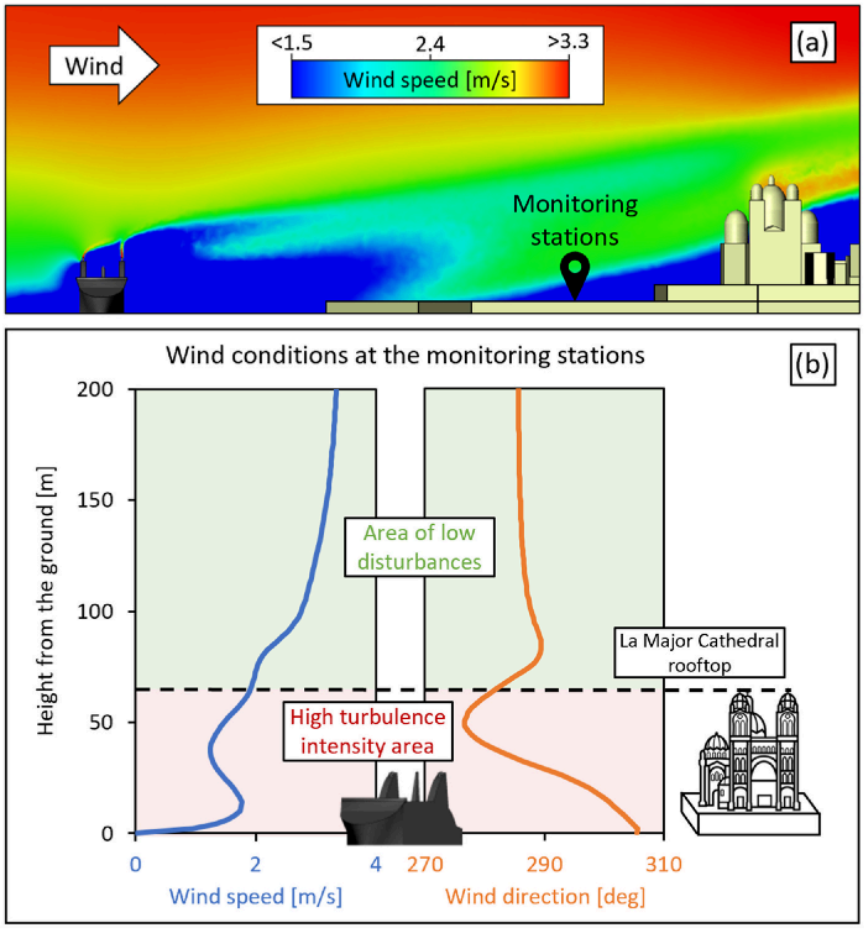

Fig. 6. Predicted wind field from the CFD model for Case 2. (a) Wind speed contour plot on a plane parallel to the plume direction, and vertical to the sea surface, crossing the vessel's funnels; (b) Vertical wind speed and wind direction profiles at the monitoring stations.

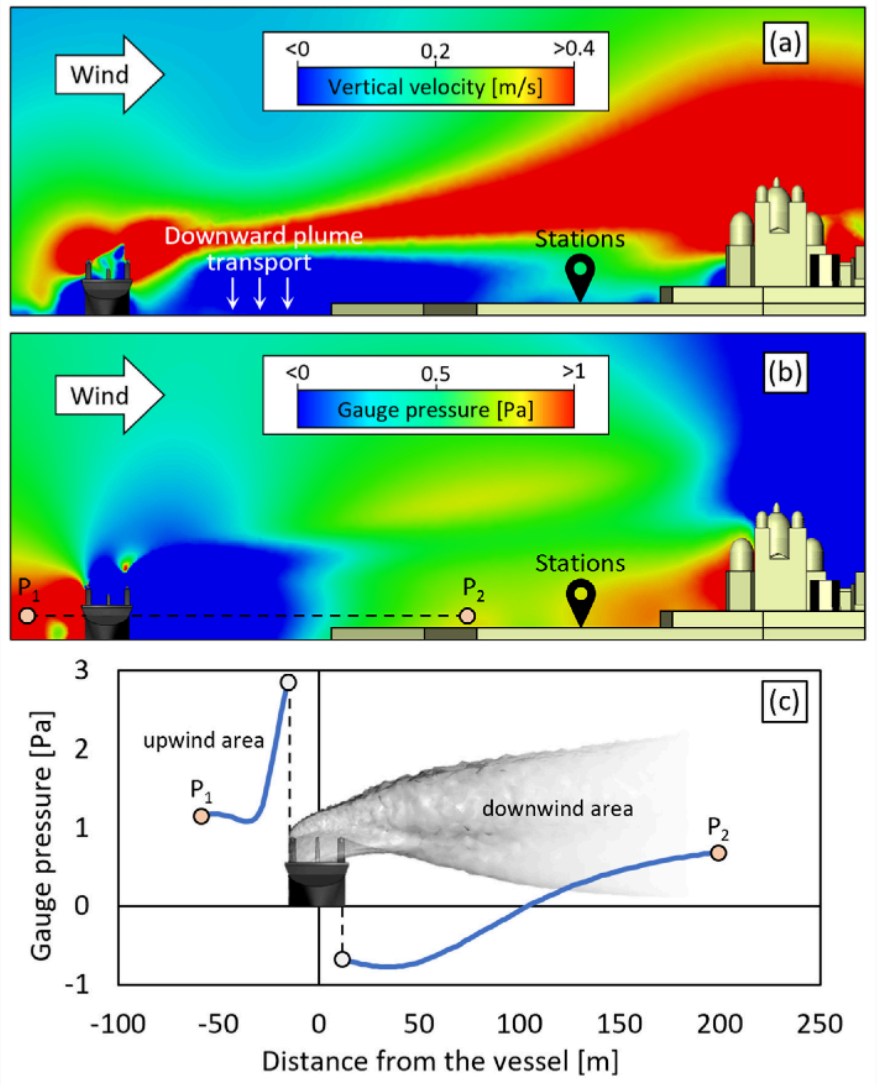

Fig. 7. Contour plots (Case 2) on a plane parallel to the plume path, and vertical to the sea surface, crossing the vessel's funnels for (a) the vertical wind velocity component and (b) gauge pressure; (c) Gauge pressure plot along the P_1–P_2 line that is 15 m above the sea level.

with gray color and includes all volume cells with SO_2 content higher than 1 ppb [v/v]. The plume cross-section area has a narrow shape close to the funnel and widens as the distance from the source increases, indicating the dispersion of the pollutants. The SO_2 content in point A is 99.5 ppm and it is diluted 100 times reaching 0.99 ppm within 170 m in point B. The CFD model predicts the SO_2 content to be 0.32 ppm and 0.16 ppm at points C and D, respectively. Cross sections B, C and D show the SO_2 contour plots which are vertical to the ground and to the main direction of the plume transport. It is observed that the distribution of SO_2 on the cross-sections is strongly affected by the surrounding buildings and urban structures. In cross-section B, SO_2 distribution is mainly concentrated around point B. In contrast, in sections C and D, SO_2 distribution shape is strongly affected by the shape of the Cathedral dome, which is the first major building downwind of the vessel. The plume elevation curve (blue line) displays the height at which the highest concentration of SO_2 occurs along the plume. Point A corresponds to the average funnel height which in the graph is set as the zero-height point. Plume elevation increases as it approaches the urban area. This behaviour can be attributed to the presence of buildings that create pressure gradients driving the plume above the city canopy.

Fig. 9a presents the contour plot of SO_2 content on a plane parallel to the ground at the height of the stations' sampling points. For the purposes of this analysis, in Fig. 6 we consider that the Virtual Sampling Point (VSP) of the CFD model is in the middle of the two actual sampling points. A typical vessel-VSP distance is 250–300 m. Positive y and x directions correspond to North and East cardinal points, respectively, and positive z direction to the zenith direction. Increased SO_2 content is observed in an area around 150 m downwind of the vessel. The wind is of northwest direction, which is almost perpendicular to the vessel, leading to low levels of pressure and velocity on its back side. The low-pressure field in this area results in an increased recirculation level, which in the end leads to high SO_2 concentration.

An important aspect that should also be examined in the model is its spatial sensitivity. In Fig. 9b, the distribution of SO_2 along the A-B line is plotted with a spatial resolution equal to the average cell size around VSP (4.6 m), to depict the variation of the CFD results in the vicinity of the monitoring stations. It is observed that within a two-cell-size distance, SO_2 content ranges from 10.1 ppb to 19.7 ppb, which is a 96% difference (black points). Correspondingly, Fig. 9c presents the vertical distribution of SO_2 at the VSP. The SO_2 content in the points below and above VSP is 9.5 ppb and 25.2 ppb, respectively. From this example, it is understood that the CFD model exhibits high variance within the order

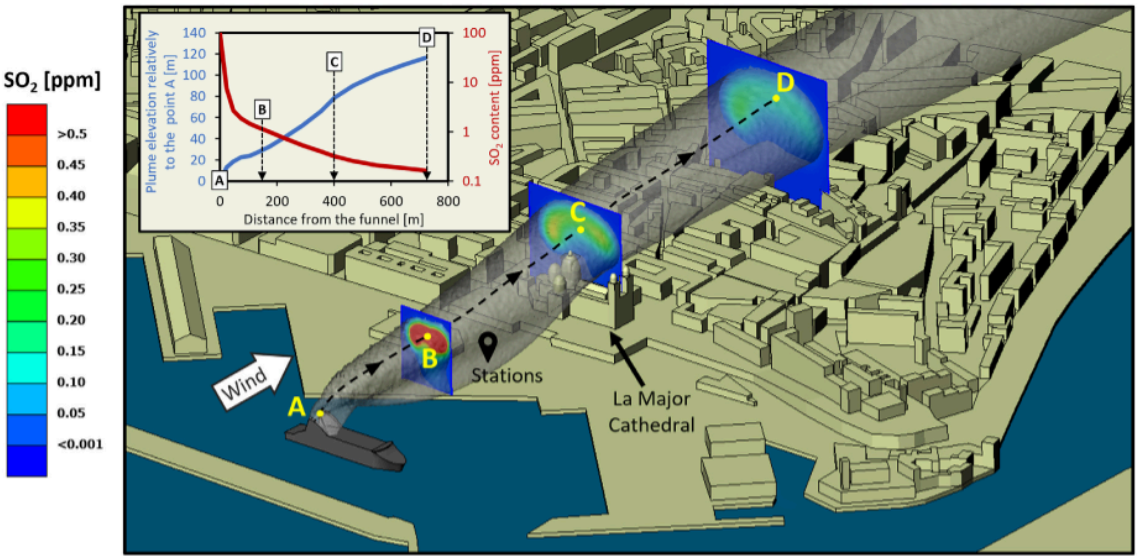

Fig. 8. Evolution and elevation of the plume emitted by the departing vessel of Case 2 in the port of Marseille, depicted through contour plots of SO_2 content in three distinct cross-sections.

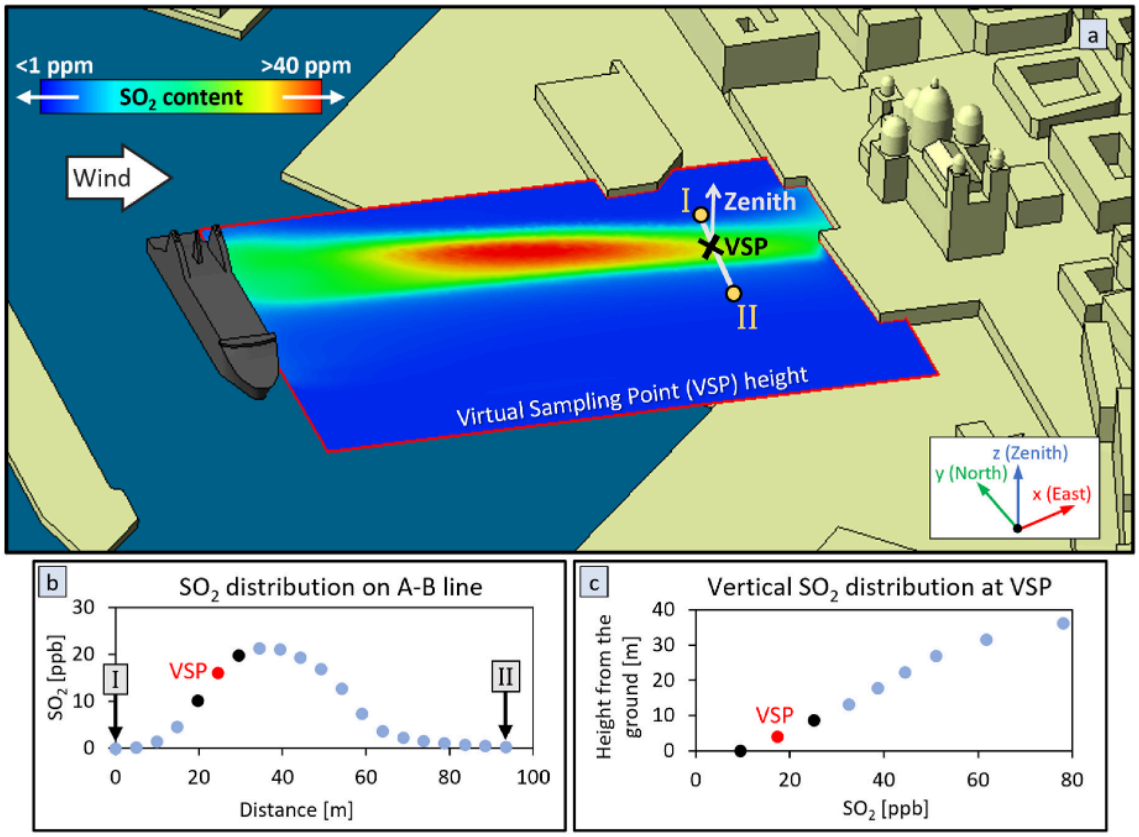

Fig. 9. Spatial sensitivity of the CFD model (Case 2). (a) SO_2 contour plot on an XY plane parallel to the sea, at the height of the sampling points; (b) spatial SO_2 distribution along the A-B line; (c) Vertical SO_2 distribution at the Virtual Sampling Point (VSP).

of its spatial resolution in the studied area. However, one can say that using a finer computational meshing would result in a smaller average cell size and thus reduced variance within the spatial resolution of the CFD model. For this reason, a mesh sensitivity analysis was conducted, demonstrating that a further increase in the mesh resolution (i.e., using a finer mesh) would not yield significantly different results. Thus, in order to account for such possible spatial variations when extracting modelling results at a particular point, the estimated concentration at its adjacent cells should be considered.

3.2. Validation of the CFD model

In this section, we present an analysis of the comparison between CFD results observations in the vicinity of the monitoring station for the three plume incidences presented in section 2.6. Fig. 10 presents the comparison of CFD results with observations for each plume incidence and pollutant (CO_2, CO, NO_x, SO_2, and PM_{tot}). In Cases 1 and 3, station 2 did not distinguish SO_2 signal above the background level. Consequently, these observations were not taken into account during the evaluation of the CFD model. In station 1, no Particulate Matter (PM_{tot}) analyser was installed, so CFD predictions were compared only to the measurements of station 2. One can first observe that, in most cases, the CFD predictions and the measurements are of the same order of magnitude for both monitoring stations. Specifically, the predictions displayed an average deviation of 8.2% (95% CI: −9.3%, 25.7%) from the measurements, when all pollutants are lumped together. To put this into perspective, the observations between the two stations differed by 5.3% (95% CI: −16.3%, 26.9%). This deviation can be partially attributed to the slightly different positions of the sampling points and to possible experimental differences between the instruments of the two stations.

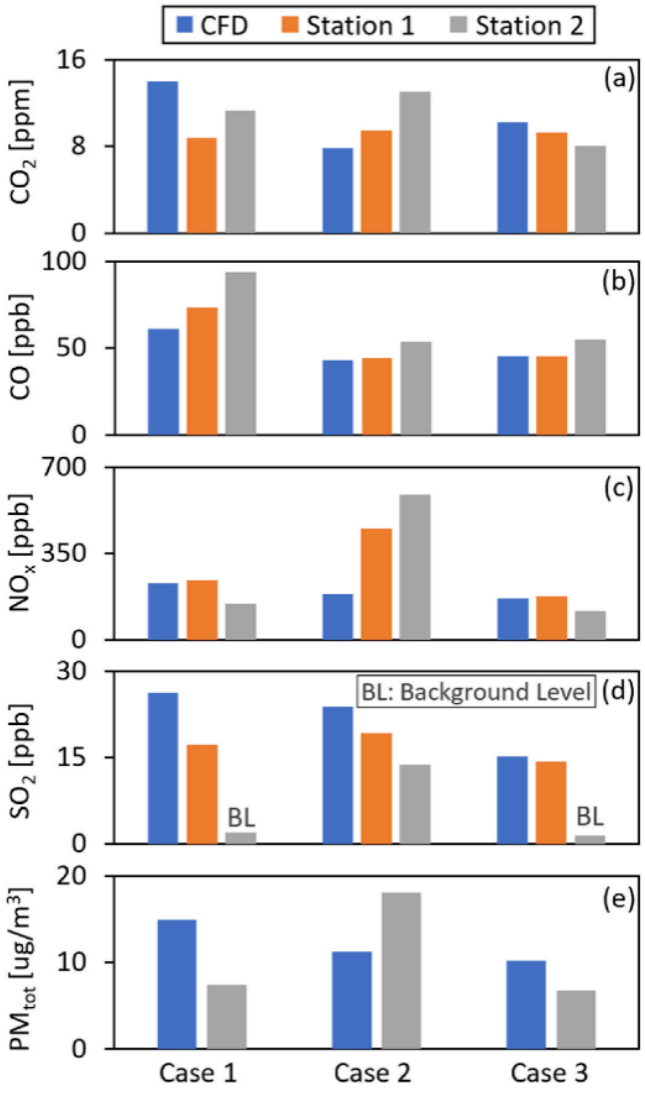

Fig. 10. Comparison of the CFD concentrations with the measured concentrations at the two different monitoring stations for Cases 1–3 for (a) CO_2, (b) CO, (c) NO_x, (d) SO_2, and (e) PM_{tot}.

When compared to the observed data, the CFD model displayed varying prediction tendencies for different pollutants within the same case. For instance, in case 1, the model overpredicted CO_2, SO_2, and PM_{tot} concentrations, underpredicted CO concentration, while NO_x predictions fell within the observations from the two stations. This behaviour cannot be solely attributed to the CFD model or assumptions such as combustion stoichiometry and engine load, but rather indicates the potential influence of inaccurate or insufficiently validated emission factors (Efs) for individual pollutants and vessels. Overall, the CFD model demonstrated acceptable deviation from the observed values without a clear bias of underestimation or overestimation.

To further evaluate the results produced from an air quality model, several validation metrics have been proposed in the literature. These metrics are mathematical expressions that compare modelling predictions (P) with observations (O), which in this study correspond to the CFD results and the measurements. The included validation metrics are the Factor of 2 (FAC2), Fractional Bias (FB), Geometric Mean Bias (MG), Normalized Mean Square Error (NMSE), and Geometric Variance (VG). The mathematical expressions for calculating these metrics are presented in the appendix of this document.

Table 2 presents the values of validation metrics for all test cases and pollutants. The acceptable range for each validation metric is described by Hanna et al. (2004) and Hanna and Chang (2012) and it is, also, reported in Table 2. CO_2 metrics are, generally, in closer proximity to their ideal values, compared to the rest of the pollutants. Since CO_2 emissions are directly proportional to fuel consumption and combustion stoichiometry, the satisfactory CO_2 metrics validate that assumptions regarding the air-to-fuel ratio and engine load factor were effectively implemented. For sulphur dioxide (SO_2) and carbon monoxide (CO), all metric values are within the acceptable range. FAC2, NMSE, and VG presented their maximum deviation for NO_x and PM_{tot}. In case 2, there was a greater deviation between the predictions and observations of nitrogen oxides (NO_x) at both monitoring stations, which led to a lower average metric value. This deviation could be attributed to the estimation of a low emission factor (EF) of NO_x for case 2. Besides, for cases 1 and 3 a good agreement between CFD predictions and measurements was observed. For the Particulate Matter (PM_{tot}) 1-min sampling average was done, while the pollutant signal lasted less than 6 min for all cases. This means that the measured PM_{tot} signal had low temporal resolution (6 temporal points at most). Therefore, in the highest 20% of PM_{tot} observations, there was only a single highest value, and no actual averaging took place, which in turn led to higher deviation between the CFD results and the measurements. In this work, all pollutants were considered to be gaseous species. This approach can be acceptably applied to CO_2, CO, NO_x and SO_2. However, PM_{tot} consists of a particulate phase, and, ideally, it should be modelled as a suspension of individual particles. To apply the proposed method more broadly, all pollutants were treated as gaseous substances with an average kinematic viscosity. Be that as it may, this assumption yielded results that were in reasonable agreement with measurements, even for the Particulate Matter.

Table 2
Statistical metrics of all test cases for CO_2, CO, NO_x, SO_2 and PM_{tot} that compare predictions and observations, used for validating the CFD model.

Metric	CO_2	CO	NO_x	SO_2	PM_{tot}	Ideal	Accepted range (Hanna and Chang, 2012; Hanna et al., 2004)
FAC2	1	1	0.67	1	0.67	1	$0.3 \leq FAC2 \leq 1$
FB	−0.11	0.24	0.25	−0.34	−0.25	0	$-0.67 < FB < 0.67$
MG	0.96	1.20	1.27	0.76	0.81	1	$0.7 < MG < 1.3$
NMSE	0.14	0.12	0.40	0.21	0.46	0	NMSE<6
VG	1.09	1.04	1.45	1.11	1.34	1	$VG < 1.6$

The resulting metric values were also compared to another research work. Toscano et al. (2021) studied the impact of cruise ship emissions in the port of Naples, using a microscale CFD and an operational air quality model. They compared the modelling predictions with wind tunnel experiments, applying some of the validation metrics used in this work. For the CFD model, NMSE ranged between 0.17 and 0.29, FAC2 between 0.625 and 0.651, and |FB| between 0.097 and 0.122. In the current work, most metric values lie within the same acceptable range. Given uncertainties, such as the engine power and the engine load, the stoichiometry of the combustion, the real FSC, the exhaust funnel temperature and the exact pollutant emission rates, the current CFD approach can reliably reproduce shipping plume dispersion within an urban area close to a port.

4. Discussion and conclusions

In this paper, a RANS CFD method for shipping emissions dispersion modelling in a port area was presented. The port of Marseille was used as a case study. The comparison of the CFD predictions with measurements for five pollutants (CO_2, CO, NO_x, SO_2, and PM) indicated that the model can reliably represent shipping emission incidents while reducing the computational cost and complexity of the modelling setup, which can make the application of this model more affordable.

To illustrate a practical application of the proposed method, we consider a scenario involving a departing Ro-Ro vessel. The vessel's length and width are 165 m and 29 m, respectively, while the funnel is 32.8 m above sea level. The installed power is 19.7 MW for the main engines and 3.9 MW for the auxiliary engines. The mass flow of the exhaust gases and the SO_2 are 10.7 kg/s and 0.01 kg/s, respectively. The wind direction is southwest (243°).

Fig. 11a shows the contour plot of SO_2 concentration on a plane 15 m above sea level. A highly polluted area is observed approximately 100 m downwind of the vessel, where the SO_2 concentration exceeds 40 μg/m^3. The opposite wind and vessel directions favour the downward plume dispersion on the vessel's rear side, resulting in high pollution levels. An additional region with high SO_2 concentration is identified within a city street canyon 1 km downwind of the vessel. Several factors contribute to the entrapment of the plume within this street canyon, including the gradual increase in ground elevation, the plume's movement towards the city, and the positioning and orientation of the buildings in this area. Fig. 11b presents the vertical distribution of SO_2 in front of two buildings within the street canyon, where the concentration ranges from 14 to 42 μg/m^3. The significant variation in concentration is attributed to the presence of intense recirculation phenomena commonly observed in such areas. Due to the increased distance of this street canyon from the vessel, it becomes challenging to directly attribute a possible high-concentration level to this specific departing vessel. However, by employing the CFD model, it is possible to establish a correlation between this pollution hotspot within the street canyon and the emissions from the vessel.

From a societal perspective, the presented model has the potential to provide valuable insights into managing ship emissions in port areas. By

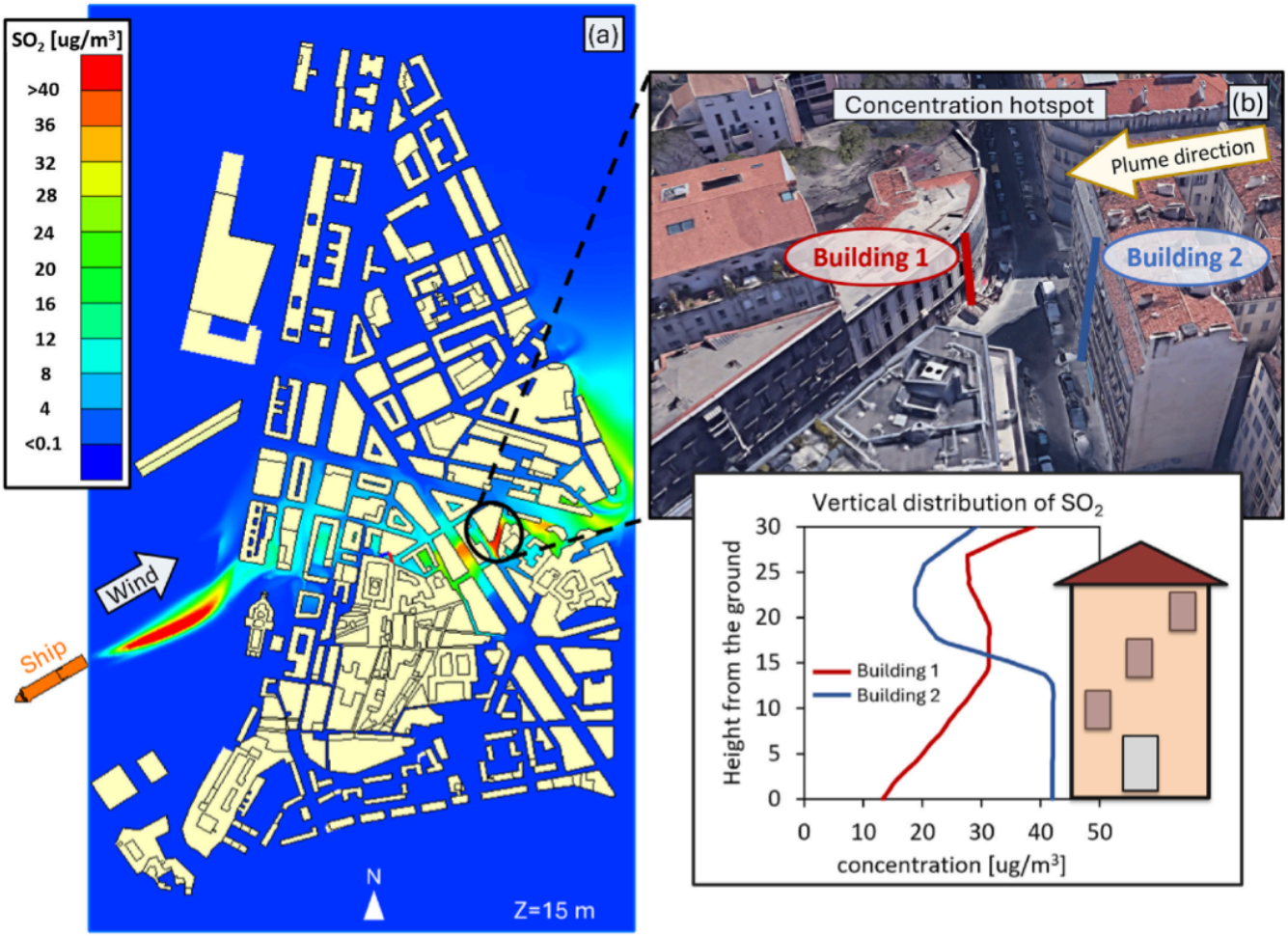

Fig. 11. Application of the proposed method on a hypothetical scenario to track concentration hot spots inside the city. (a) Contour plot of SO_2 concentration on a plane 15 m above the sea level; (b) Vertical SO_2 distribution in front of two buildings, at a street canyon where the vessel's plume has been entrapped.

simulating the dispersion of ship plumes, local authorities can identify high-pollution areas and apply emission reduction measures, such as using cleaner fuels or implementing cold ironing strategies, if need be. Furthermore, the model can evaluate the effectiveness of different emission reduction measures under different scenarios, allowing local authorities to choose the most effective ones.

The CFD model can also provide information about the complex wind airflow patterns that dominate inside an urban environment and determine the dispersion of pollutants, by tracking areas with high recirculation levels, as seen in Fig. 11. This kind of knowledge could contribute to the improvement of urban and land-use planning, favouring the ventilation of street canyons and improving the air quality in them. For example, the application of this model can assist local authorities decide the location of a hospital or a school, in order to reduce the exposure of patients and students to hazardous pollutants.

In conclusion, the presented CFD model can be a reliable and valuable tool for port authorities and policymakers to manage shipping emissions in port areas. The model can realistically reproduce the dispersion of shipping-emitted plumes, identify high-pollution areas, prioritize emission reduction measures, and evaluate the effectiveness of different measures under different scenarios. Finally, it can potentially contribute to urban planning with a view to minimizing the exposure of vulnerable citizens to hazardous pollutants.

Future research could also include parametric sensitivity analysis and other pollution sources. A sensitivity analysis on different parameters such as exhaust gas emission conditions, vessel position, funnel height, wind conditions, can be conducted using the current CFD method to investigate their impact on air pollution. Moreover, a comparative analysis between different emission sources will provide a better insight into how shipping activity contributes to the air pollution of port areas.

CRediT authorship contribution statement

Christos Boikos: Conceptualization, Methodology, Software, Validation, Formal analysis, Investigation, Data curation, Writing – original draft, Writing – review & editing, Visualization. **Panagiotis Siamidis:** Methodology, Software, Formal analysis, Investigation, Data curation, Visualization. **Sonia Oppo:** Methodology, Software, Formal analysis, Resources, Data curation, Writing – review & editing. **Alexandre Armengaud:** Methodology, Resources, Data curation, Writing – review & editing. **George Tsegas:** Methodology, Data curation, Writing – review & editing. **Johan Mellqvist:** Methodology, Resources, Data curation, Writing – review & editing. **Vladimir Conde:** Methodology, Resources, Data curation, Writing – review & editing. **Leonidas Ntziachristos:** Conceptualization, Methodology, Resources, Writing – original draft, Writing – review & editing, Supervision.

Declaration of competing interest

The authors declare the following financial interests/personal relationships which may be considered as potential competing interests: Christos Boikos reports financial support was provided by the Hellenic Foundation for Research and Innovation under the 3rd Call for HFRI PhD Fellowships (Fellowship Number: 6316).

Data availability

Data will be made available on request.

Acknowledgements

The research work was supported by the Hellenic Foundation for Research and Innovation (HFRI) under the 3rd Call for HFRI PhD Fellowships (Fellowship Number: 6316).

The 3D plan of the building geometry of Marseille and the observed pollutant timeseries were gained in the context of the EU HORIZON 2020 Project, SCIPPER (Grant agreement ID: 814893). Ship trajectories and timestamps were obtained from an AIS database provided by the 'exactEarth Europe LTD'.

Appendix

In this section the validation metrics used for the evaluation of the CFD model according to Hanna et al. (2004) are presented. The predicted concentrations are symbolized with C_p, while observations with C_o. The overbar $\overline{C}$ means the average over the dataset.

The Fractional Bias (FB) shows the linear average bias:

$$FB = \frac{(\overline{C}_o - \overline{C}_p)}{0.5 \cdot (\overline{C}_o + \overline{C}_p)}$$

The Geometric Mean Bias (MG) shows the logarithmic average bias:

$$MG = \exp(\overline{\ln C_o} - \overline{\ln C_p})$$

The Normalized Mean Square Error (NMSE) is an indicator of data scattering, which contains systematic and random errors:

$$NMSE = \frac{\overline{(C_o - C_p)^2}}{\overline{C}_o \cdot \overline{C}_p}$$

Geometric Variance (VG) shows data scattering in a logarithmic scale which contains systematic and random errors:

$$VG = \exp\left[\overline{(\ln C_o - \ln C_p)^2}\right]$$

The Factor of 2 (FAC2) is the fraction of predictions within a factor of two of observations:

$$FAC2 = \textit{fraction of data that satisfy } 0.5 \leq \frac{C_p}{C_o} \leq 2$$

References

Amorim, J.H., Rodrigues, V., Tavares, R., Valente, J., Borrego, C., 2013. CFD modelling of the aerodynamic effect of trees on urban air pollution dispersion. Sci. Total Environ. 461, 541–551. https://doi.org/10.1016/j.scitotenv.2013.05.031. –462.

ANSYS Inc, 2021. ANSYS Fluent 2022 R1, Theory Guide, https://ansyshelp.ansys.com/account/secured?returnurl=/Views/Secured/prod_page.html?pn=Fluent&prodver=22.1&lang=en.

Badeke, R., Matthias, V., Grawe, D., 2021. Parameterizing the vertical downward dispersion of ship exhaust gas in the near field. Atmos. Chem. Phys. 21, 5935–5951. https://doi.org/10.5194/acp-21-5935-2021.

Balzani Lööv, J.M., Alfoldy, B., Gast, L.F.L., Hjorth, J., Lagler, F., Mellqvist, J., Beecken, J., Berg, N., Duyzer, J., Westrate, H., Swart, D.P.J., Berkhout, A.J.C., Jalkanen, J.P., Prata, A.J., Van Der Hoff, G.R., Borowiak, A., 2014. Field test of available methods to measure remotely SOx and NOx emissions from ships. Atmos. Meas. Tech. 7, 2597–2613. https://doi.org/10.5194/amt-7-2597-2014.

Blocken, B., 2015. Computational Fluid Dynamics for urban physics: importance, scales, possibilities, limitations and ten tips and tricks towards accurate and reliable simulations. Build. Environ. 91, 219–245. https://doi.org/10.1016/j.buildenv.2015.02.015.

Blocken, B., Gualtieri, C., 2012. Ten iterative steps for model development and evaluation applied to computational fluid dynamics for environmental fluid mechanics. Environ. Model. Software 33, 1–22. https://doi.org/10.1016/j.envsoft.2012.02.001.

Blocken, B., Vervoort, R., van Hooff, T., 2016. Reduction of outdoor particulate matter concentrations by local removal in semi-enclosed parking garages: a preliminary case study for Eindhoven city center. J. Wind Eng. Ind. Aerod. 159, 80–98. https://doi.org/10.1016/j.jweia.2016.10.008.

Bonifacio, H.F., Maghirang, R.G., Glasgow, L.A., 2014. Numerical simulation of transport of particles emitted from ground-level area source using AERMOD and CFD. Engineering Applications of Computational Fluid Mechanics 8, 488–502. https://doi.org/10.1080/19942060.2014.11083302.

Du, Y., Blocken, B., Abbasi, S., Pirker, S., 2021. Efficient and high-resolution simulation of pollutant dispersion in complex urban environments by island-based recurrence CFD. Environ. Model. Software 145. https://doi.org/10.1016/j.envsoft.2021.105172.

European Environmental Agency, 2022. Air Quality in Europe 2022. www.eea.europa.eu/publications/air-quality-in-europe-2022.

FleetMon, 2023. Accessed3.20.23 www.fleetmon.com/.

Franke, J., 2006. Recommendations of the COST action C14 on the use of CFD in predicting pedestrian wind environment. In: The Fourth International Symposium on Computational Wind Engineering (CWE2006). pp. 529–532 Yokoshama, Japan. www.iawe.org/Proceedings/CWE2006/TA4-01.pdf.

Grigoriadis, A., Mamarikas, S., Ioannidis, I., Majamäki, E., Jalkanen, J.P., Ntziachristos, L., 2021. Development of exhaust emission factors for vessels: a review and meta-analysis of available data. Atmos. Environ. X 12. https://doi.org/10.1016/j.aeaoa.2021.100142.

Hanna, S., Chang, J., 2012. Acceptance criteria for urban dispersion model evaluation. Meteorol. Atmos. Phys. 116, 133–146. https://doi.org/10.1007/s00703-011-0177-1.

Hanna, S.R., Hansen, O.R., Dharmavaram, S., 2004. FLACS CFD air quality model performance evaluation with Kit Fox, MUST, Prairie Grass, and EMU observations. Atmos. Environ. 38, 4675–4687. https://doi.org/10.1016/j.atmosenv.2004.05.041.

Haugen, M.J., Gkantonas, S., el Helou, I., Pathania, R., Mastorakos, E., Boies, A.M., 2022. Measurements and modelling of the three-dimensional near-field dispersion of particulate matter emitted from passenger ships in a port environment. Atmos. Environ. 290, 119384 https://doi.org/10.1016/j.atmosenv.2022.119384.

Holmes, N.S., Morawska, L., 2006. A review of dispersion modelling and its application to the dispersion of particles: an overview of different dispersion models available. Atmos. Environ. 40, 5902–5928. https://doi.org/10.1016/j.atmosenv.2006.06.003.

International Maritime Organization, 2016. Marpol annex VI, sulphur oxides (SOx) and particulate matter (PM) – regulation 14. Resolution MEPC 280 (70). www.imo.org/en/OurWork/Environment/Pages/Sulphur-oxides-(SOx)-%E2%80%93-Regulation-14.aspx.

International Maritime Organization, 2014. MARPOL Annex VI, Nitrogen Oxides (NOx) – Regulation 13. www.imo.org/en/OurWork/Environment/Pages/Nitrogen-oxides-(NOx)-%E2%80%93-Regulation-13.aspx.

Jaffe, L.S., 1968. Ambient carbon monoxide and its fate in the atmosphere. J. Air Pollut. Control Assoc. 18, 534–540. https://doi.org/10.1080/00022470.1968.10469168.

Karl, M., Bieser, J., Geyer, B., Matthias, V., Jalkanen, J.P., Johansson, L., Fridell, E., 2019. Impact of a nitrogen emission control area (NECA) on the future air quality and nitrogen deposition to seawater in the Baltic Sea region. Atmos. Chem. Phys. 19, 1721–1752. https://doi.org/10.5194/acp-19-1721-2019.

Li, J., Song, J., Xu, Y., Yu, Q., Zhang, Y., Ma, W., 2022. Parameterization of a rising smoke plume for a large moving ship based on CFD. Atmosphere 13, 1507. https://doi.org/10.3390/atmos13091507.

Li, X.B., Lu, Q.C., Lu, S.J., He, H. di, Peng, Z.R., Gao, Y., Wang, Z.Y., 2016. The impacts of roadside vegetation barriers on the dispersion of gaseous traffic pollution in urban street canyons. Urban For. Urban Green. 17, 80–91. https://doi.org/10.1016/j.ufug.2016.03.006.

Long, B., Bao, J.L., Truhlar, D.G., 2017. Reaction of SO2 with OH in the atmosphere. Phys. Chem. Chem. Phys. 19, 8091–8100. https://doi.org/10.1039/c7cp00497d.

Matthias, V., Bewersdorff, I., Aulinger, A., Quante, M., 2010. The contribution of ship emissions to air pollution in the North Sea regions. Environ. Pollut. 158, 2241–2250. https://doi.org/10.1016/j.envpol.2010.02.013.

Mayeli, P., Sheard, G.J., 2021. Buoyancy-driven flows beyond the Boussinesq approximation: a brief review. Int. Commun. Heat Mass Tran. 125 https://doi.org/10.1016/j.icheatmasstransfer.2021.105316.

Ntziachristos, L., Saukko, E., Lehtoranta, K., Rönkkö, T., Timonen, H., Simonen, P., Karjalainen, P., Keskinen, J., 2016. Particle emissions characterization from a medium-speed marine diesel engine with two fuels at different sampling conditions. Fuel 186, 456–465. https://doi.org/10.1016/j.fuel.2016.08.091.

Oldrini, O., Armand, P., Duchenne, C., Perdriel, S., 2019. Parallelization performances of PMSS flow and dispersion modeling system over a huge urban area. Atmosphere 10. https://doi.org/10.3390/atmos10070404.

Pan, K., Lim, M.Q., Kraft, M., Mastorakos, E., 2021. Development of a moving point source model for shipping emission dispersion modelling in EPISODE-CityChem v1.3. Geosci. Model Dev. (GMD) 14, 4509–4534. https://doi.org/10.5194/gmd-2021-47.

Rapkos, N., Weigelt, A., Beecken, J., Ntziachristos, L., 2023. Method to identify fuel sulphur content (FSC) violations of ongoing vessels using CFD modelling. Atmos. Environ. 309 https://doi.org/10.1016/j.atmosenv.2023.119912.

Ricci, A., Kalkman, I., Blocken, B., Burlando, M., Repetto, M.P., 2020. Impact of turbulence models and roughness height in 3D steady RANS simulations of wind flow in an urban environment. Build. Environ. 171 https://doi.org/10.1016/j.buildenv.2019.106617.

Sanchez, B., Santiago, J.L., Martilli, A., Martin, F., Borge, R., Quaassdorff, C., de la Paz, D., 2017. Modelling NOX concentrations through CFD-RANS in an urban hot-spot using high resolution traffic emissions and meteorology from a mesoscale model. Atmos. Environ. 163, 155–165. https://doi.org/10.1016/j.atmosenv.2017.05.022.

Santiago, J.L., Martín, F., Martilli, A., 2013. A computational fluid dynamic modelling approach to assess the representativeness of urban monitoring stations. Sci. Total Environ. 454, 61–72. https://doi.org/10.1016/j.scitotenv.2013.02.068. –455.

Tominaga, Y., Mochida, A., Yoshie, R., Kataoka, H., Nozu, T., Yoshikawa, M., Shirasawa, T., 2008. AIJ guidelines for practical applications of CFD to pedestrian wind environment around buildings. J. Wind Eng. Ind. Aerod. 96, 1749–1761. https://doi.org/10.1016/j.jweia.2008.02.058.

Tominaga, Y., Stathopoulos, T., 2016. Ten questions concerning modeling of near-field pollutant dispersion in the built environment. Build. Environ. 105, 390–402. https://doi.org/10.1016/j.buildenv.2016.06.027.

Toscano, D., Marro, M., Mele, B., Murena, F., Salizzoni, P., 2021. Assessment of the impact of gaseous ship emissions in ports using physical and numerical models: the case of Naples. Build. Environ. 196 https://doi.org/10.1016/j.buildenv.2021.107812.

Toscano, D., Murena, F., Quaranta, F., Mocerino, L., 2022. Impact of ship emissions at a high receptor point in the port of Naples. Atmos. Environ. 286, 119253 https://doi.org/10.1016/j.atmosenv.2022.119253.

United Nations. World Urbanization Prospects: the 2018 Revision. www.un.org/en/desa/2018-revision-world-urbanization-prospects.

U.S. Environmental Protection Agency, 2009. Current Methodologies in Preparing Mobile Source Port-Related Emission Inventories Final Report.

Viana, M., Hammingh, P., Colette, A., Querol, X., Degraeuwe, B., Vlieger, I. de, van Aardenne, J., 2014. Impact of maritime transport emissions on coastal air quality in Europe. Atmos. Environ. https://doi.org/10.1016/j.atmosenv.2014.03.046.

Wang, S., Wang, X., 2019. Modeling and analysis of noise barrier shape effects on highway automobiles emission dispersion. In: ASME International Mechanical Engineering Congress and Exposition, Proceedings (IMECE). American Society of Mechanical Engineers (ASME). https://doi.org/10.3390/fluids4030151.